Dynamics of soap bubble bursting and its implications to volcano acoustics

Valérie Vidal, Maurizio Ripepe, Thibaut Divoux, Denis Legrand, Jean-Christophe Géminard, Francisco Melo

Dynamics of soap bubble bursting and its implications to volcano acoustics

V. Vidal[1,2], M. Ripepe[3], T. Divoux[1], D. Legrand[4,5], J.-C. Géminard[1,2], and F. Melo[1]

[1]Laboratorio de Física No Lineal and CIMAT, Departamento de Física,
Universidad de Santiago de Chile, Avenida Ecuador 3493, Santiago, Chile.

[2]Laboratoire de Physique, Université de Lyon, Ecole Normale Supérieure - CNRS,
46 Allée d'Italie, 69364 Lyon Cedex 07, France.

[3]Dipartimento di Scienze della Terra, Università degli Studi di Firenze,
via La Pira, 4 - 50121 Firenze, Italy.

[4]Universidad de Chile, Departamento de Geofísica, Blanco Encalada 2002, Santiago, Chile.

[5]Now at: Universidad Autónoma de México, Ciudad Universitaria, Instituto
de Geofísica, Departamento de Vulcanología, Del. Coyoacan, CP 04510, México DF.

April 9, 2010

Abstract

In order to assess the physical mechanisms at stake when giant gas bubbles burst at the top of a magma conduit, laboratory experiments have been performed. An overpressurized gas cavity is initially closed by a thin liquid film, which suddenly bursts. The acoustic signal produced by the bursting is investigated. The key result is that the amplitude and energy of the acoustic signal strongly depend on the film rupture time. As the rupture time is uncontrolled in the experiments and in the field, the measurement of the acoustic excess pressure in the atmosphere, alone, cannot provide any information on the overpressure inside the bubble before explosion. This could explain the low energy partitioning between infrasound, seismic and explosive dynamics often observed on volcanoes.

1 Introduction

Volcanic explosions generate both seismic and acoustic waves propagating in the ground and in the atmosphere, respectively. Monitoring the acoustic emissions thus represents, together with the seismic signals monitoring, an attractive tool to investigate the source of volcanic explosions. In particular, the simultaneous recording of the seismic and acoustic signals might provide clues to constrain the source process (e.g. [*Vergniolle and Brandeis* (1996)]). However, the link between the seismic and acoustic waves and the explosive source dynamics is still poorly understood. Some authors claim that seismic and acoustic waves are generated by an unique shallow process ($<$ 500 m depth) [*Kobayashi et al.* (2005), *Johnson* (2007)]. Others propose that the acoustic waves are produced by the bursting of meter-sized gas bubbles, while the seismic waves result from the pressure variations, in the magma column, associated with the rise of the gas bubbles toward the surface [*Ripepe et al.* (2001), *Chouet et al.* (2003), *James et al.* (2004)]. Nonetheless, almost all studies assert that acoustic waves are generated either by the bursting of the gas bubbles [*Ripepe et al.* (1996), *Johnson* (2003)] or by the oscillation of the magma membrane covering the gas slug just before the burst-

ing [*Vergniolle and Brandeis* (1996)].

The acoustic wave characteristics, in the infrasonic range, are commonly related to the properties of the bursting bubble, such as its volume and overpressure before bursting [*Vergniolle and Brandeis* (1996)]. However, most of these analysis are theoretical and numerical (e.g. [*Vergniolle and Brandeis* (1996)]). Only a few laboratory experiments were dedicated to characterizing the acoustics of bubble bursting in conditions that are relevant to volcanology [*James et al.* (2004), *James et al.* (2009)].

Here we investigate experimentally the bursting, in static conditions, of a 'slug' whose parameters (geometry and overpressure) are accurately controlled. The characteristics of the acoustic signal emitted at bursting (frequency, energy) are compared with the initial bubble geometry (volume) and overpressure. This experiment focuses on the physical mechanisms at stake when the overpressurized cavity suddenly opens. Because the dynamics of bubble bursting on volcanoes is much more complex, we will not compare directly our experiment with the field situation. However, the physical processes we describe here are likely to be involved when a large gas bubble explodes at the top of a volcano vent (Figure 1a). We therefore comment the results in regard to potential implications for large bubbles bursting on volcanoes. We discuss further (section 5) the limits of this application.

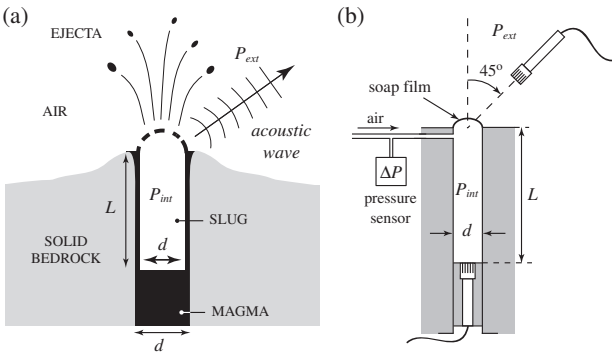

Figure 1: (a) Sketch of a slug exploding at the top of a volcanic conduit. b) Experimental setup of a soap film bursting at the surface of a cavity of well controlled geometry (length L, diameter d, volume V) and initial overpressure (ΔP).

2 Experimental results

Our experimental setup consists of a cylindrical cavity drilled in a plexiglas slab (Figure 1b). Following [*Vidal et al.* (2006)], we close the cavity by stretching a thin soap film. Air is injected inside and, due to the increase in the inner pressure, the thin soap film deforms and bulges out. Injection is stopped when a chosen overpressure ΔP is reached. The system then remains in mechanical equilibrium, while the soap film drains the liquid aside [*Mysels et al.* (1959)] and eventually bursts. This controlled experiment makes possible to easily vary the length and volume of the cavity, and the gas overpressure before the film bursting. Different tube lengths L (from 2 to 23 cm) and diameters d (6, 8 or 10 mm) have been used (aspect ratio $\alpha = L/d$ ranging from 2 to 23) in order to quantify the role of the conduit geometry.

The rupture of the film results in a sudden drop of the inner overpressure, which excites resonant modes inside the cavity. The inner standing waves are damped due to dissipation along the walls and radiation out of the open end of the cavity. A microphone inside the tube (Figure 1b, bottom) records the pressure variation at the cavity bottom (P_{int}) while a microphone outside (Figure 1b, top) monitors the radiated acoustic waves (P_{ext}). As expected for a resonating tube, both signals, inside and outside, exhibit the same spectral content, with a fundamental frequency associated with the wavelength in air $\lambda_0 \sim 4L$ and odd harmonics [*Kinsler et al.* (1982)]. Note that the location of the inner microphone is pertinent, as the amplitude of the pressure variation associated with all the harmonics is maximum at the cavity bottom.

3 Partitioning of the acoustic pressure

When the soap film breaks at the top of the cavity, the overpressure recorded by the bottom microphone

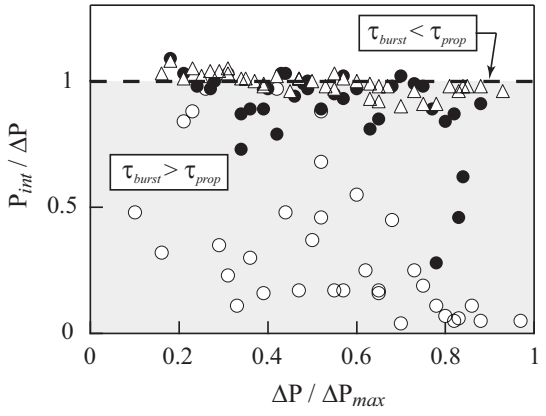

Figure 2: Normalized amplitude $P_{int}/\Delta P$ of the acoustic signal at bursting, inside the cavity, as a function of the initial normalized overpressure $\Delta P/\Delta P_{max}$. $P_{int}/\Delta P < 1$ (gray region) indicates a slow dynamics of the film opening. [Symbol,α]: [$\circ$,2]; [$\bullet$,8]; [$\triangle$,23].

(Figure 1b) drops from $+\Delta P$ to $-P_{int}$. Before the bursting, the overpressure ΔP inside the cavity is constant. We thus expect, in the absence of significant energy loss, to measure $P_{int} = \Delta P$. We found that this is true only for long tubes ($\alpha = 23$, large gas volume) whereas for short tubes ($\alpha = 2$, small gas volume) a large scatter of the pressure drop is observed, with $P_{int} \leq \Delta P$ (Figure 2).

This scatter can be explained by taking into account the film rupture dynamics, and in particular its typical rupture time τ_{burst} [*Vidal et al.* (2006), *Divoux et al.* (2008)]. It is approximated, from the experimental data, as the time necessary for the overpressure at the cavity bottom to drop from $+\Delta P$ to $-P_{int}$. The characteristic film rupture time is compared to the propagation time τ_{prop} of the acoustic wave inside the tube, defined as

$$\tau_{prop} = 2L/c \qquad (1)$$

where c is the sound velocity ($c = 340$ m/s). The experiment indicates that the initial relative amplitude $P_{int}/\Delta P$ is a strongly decreasing function of the ratio τ_{burst}/τ_{prop} (Figure 3a). In other words, for a given geometry, the larger the characteristic rupture time is, the smaller is the amount of energy transferred to the resonant modes [*Vidal et al.* (2006)]. For $\tau_{burst}/\tau_{prop} > 1$, we observe a drastic drop in the amplitude P_{int} of the signal inside the cavity. Long cavities (large aspect ratio, e.g. $\alpha = 23$) are not sensitive to the film rupture time, as they always fulfill the condition $\tau_{burst} < \tau_{prop}$. In this case, the acoustic amplitude inside the tube well approaches the initial overpressure, and $P_{int}/\Delta P \simeq 1$ (Figures 2 and 3a). To the contrary, for short cavities, the system is sensitive to the film rupture time, which is on the order of τ_{prop}, and a large scatter is observed. The uncontrolled bubble rupture time thus accounts for the scatter of the acoustic energy measured outside the cavity (P_{ext}, see section 4).

On volcanoes, we do not have access to the acoustic waves inside the slug, and we measure the acoustic signal propagating outside. When a slug bursts, part of the energy is radiated as infrasonic waves in the atmosphere, while part remains trapped in the volcanic body and propagates as seismic waves. We consider here that the overpressure recorded by the internal microphone (P_{int}, Figure 1b) represents the amplitude (and/or the energy) of the seismic signal generated by the explosive process, while the pressure outside the cavity (P_{ext}) is comparable to the amplitude of the acoustic waves recorded in the atmosphere as infrasonic waves.

Therefore, by comparing the amplitude ratio between the internal and external pressure variations (Figure 3b, inset), we assume to observe a process similar to the amplitude (or energy) partitioning between seismic and acoustic waves associated with the same explosive dynamics. Our experiment indicates that the inside and outside pressure partitioning (P_{ext}/P_{int}) changes as function of the tube length and hence, of the bubble volume. Longer tubes have acoustic waves with long propagation time and with large damping effects due to viscous dissipation. As a consequence, the amplitude of the acoustic signal outside the cavity will be much smaller than for short tubes (Figure 3b, inset).

In other words, long tubes (e.g. $L = 23$ cm) are more efficient in terms of acoustic wave energy trapped inside the cavity (Figures 2 and 3a), but are not efficient to transmit acoustic energy outside (Fig-

ure 3b, inset). In contrast, short tubes (e.g. $L = 2$ cm) are more efficient in radiating acoustic energy outside (Figure 3b, inset), but are also more sensitive to the rupture time ($\tau_{burst}/\tau_{prop} > 1$, Figure 3a). If the energy loss for long tubes is mainly due to the non-efficient radiation process (small P_{ext}/P_{int}), the energy loss for short tubes (higher P_{ext}/P_{int}) is mainly due to the film rupture time ($\tau_{burst}/\tau_{prop} > 1$). In both cases, energy is dissipated.

4 Energy balance

In order to quantify the total energy balance in the system, we estimate the acoustic energy E_a from the signal measured outside:

$$E_a = \frac{2\pi r^2}{\rho c} \int_{t=0}^{\infty} P_{ext}^2(t)\, dt \qquad (2)$$

where r is the distance between the cavity aperture and the microphone, ρ the gas density, and c the sound velocity in air. The potential energy stored inside the 'slug' before bursting can be written as:

$$E_p = \frac{1}{2} \frac{V \Delta P^2}{\rho c^2} \qquad (3)$$

where V is the volume of the gas slug. Figure 4 displays the acoustic energy measured outside, as a function of the initial slug overpressure, before bursting. The three different experimental conditions represent the field situation, where the conduit radius is constant in time, but the slug length can vary from one explosion to another [*Vergniolle and Brandeis* (1996)]. We report in Figure 4 the maximum total acoustic energy estimated from a series of 10 measurements, performed in similar conditions (same ΔP). Each point then represents the acoustic energy obtained when the rupture time is the smallest. Its effect is therefore considered negligible ($\tau_{burst}/\tau_{prop} < 1$).

For small initial overpressure ΔP, the acoustic energy E_a behaves as $E_a \sim \Delta P^2$. When ΔP increases, the bubble deforms and the soap film curvature increases. Consequently, when the film bursts, the pressure front entering the cavity is spherical, and thus no longer matches the planar geometry of the resonant modes. As a consequence, the efficiency of the energy transfer decreases and E_a drops down when ΔP is increased (Figure 4). Finally, we point out that this simple bubble bursting cannot build up gas overpressure above the maximum threshold. For a bubble bursting in static condition, the threshold pressure ΔP_{max} is given by $\Delta P_{max} = 8\sigma/d$ (semispherical film), where σ represents the film surface tension.

In summary, two mechanisms limit the energy tranfer to the acoustic waves. First, the characteristic rupture time of the film breaking (section 3); Second, the film curvature before bursting. Indeed, as the film curvature increases, the pressure of the acoustic wave front generated at bursting departs from a planar wavefield. It is therefore less efficient in exciting the cavity resonant modes. This explains why, in the experiment, the fraction of energy, E_a/E_p, measured outside is small ($\sim$15%) [*Vidal et al.* (2006)], and points out the importance of the geometry and dynamics of the film rupture in controlling the amount of energy released in the atmosphere as acoustic waves.

On volcanoes, the velocity of the film rupture and the film geometry itself are much more complex than in our experiments performed in static conditions, and depend largely on the dynamics of the bubble rising and on viscosity, temperature and volatile content of the magma film layer above the bubble.

5 Discussion and Conclusion

This simple experiment provides an insight into the physical mechanisms involved in the bursting of a slug of well-controlled geometry and overpressure, in static conditions. Even in a fully controlled laboratory experiment, the amplitude and energy of the pressure wave propagating into the atmosphere after bursting cannot be predicted from the initial slug overpressure - and vice versa. We demonstrated that two processes are responsible for this unpredictability: (1) the rupture time of the bubble film, which cannot be controlled in the experiments; and (2) the energy loss due to the film curvature at bursting, which excites more or less efficiently the cavity.

When the rupture time τ_{burst} is larger than the characteristic propagation time τ_{prop} inside the cavity, the acoustic signal amplitude (and, thus, the energy) drops. The energy fraction (E_a/E_p) transferred into the acoustic signal radiated outside decreases drastically when the rupture time τ_{burst} increases.

A quantitative comparison with the much more complex field situation is out of the scope of this paper. Indeed, when a slug bubble rises and bursts in a volcanic conduit, viscous and inertial forces - two processes not investigated in this work - play an important role. On the one hand, by limiting the bubble expansion when rising, these forces are thought to be responsible for the large overpressure stored inside the slug before bursting [*James et al.* (2008)]. On the other hand, viscous effects may strongly affect the dynamics of the film aperture [*Debrégeas et al.* (1995)]. Experiments investigating bubbles bursting in either a Newtonian [*James et al.* (2008)] or non-Newtonian [*Divoux et al.* (2008)] fluids pointed out the importance of the rising velocity and, more generally, of the bursting dynamics, on the acoustic wave amplitude.

However, even if in static conditions, the physical mechanisms described here are likely to be at stake in the field. Different rupture dynamics and film thicknesses largely affect the rupture time, and the acoustic signal emitted at bursting. In particular, we point out that any interpretation of the measured acoustic amplitude, or energy, in terms of gas overpressure in the bubble before bursting requires a good knowledge of the physics controlling the opening of the bubble at bursting. This suggests that on volcanoes also, the amplitude of the acoustic waves generated by the bubble bursting strongly depends on the thickness and on the rupture velocity of the bubble cap at bursting. Both features are uncontrolled in the field, and could explain the low correlation observed at Stromboli volcano between the amplitude of the acoustic wave and the vigor of the explosive event both in terms of mass of ejected fragments [*Marchetti et al.* (2009)] and gas volume [*McGonigle et al.* (2009)].

Acknowledgments We thanks M. Ichihara for the fruitful discussions on a previous version of this manuscript. S. Lane is acknowledged for his useful comments, which improved the manuscript. D.L. was supported by FONDECYT Project #1061253. V.V., D.L., J.C.G. and F. M. were supported by CNRS/CONICYT Project #18640. V.V. and J.C.G. thank the *Centre National de la Recherche Scientifique* (CNRS, France) for supporting the research of their members in foreign laboratories.

References

[*Chouet et al.* (2003)] Chouet, B., P. Dawson, T. Ohminato, M. Martini, G. Saccorotti, F. Giudicepietro, G. De Luca, G. Milana, and R. Scarpa (2003), Source mechanisms of explosions at Stromboli Volcano, Italy, determined from moment-tensor inversions of very-long-period data, *J. Geophys. Res.*, *108*, 2019.

[*Debrégeas et al.* (1995)] Debrégeas, G., P. Martin and F. Brochard-Wyard (1995), Viscous bursting of suspended films, *Phys. Rev. Lett.*, *75*, 3886–3889.

[*Divoux et al.* (2008)] Divoux, T., V. Vidal, F. Melo and J.-C. Géminard (2008), Acoustic emission associated with the bursting of a gas bubble at the free surface of a non-Newtonian fluid, *Phys. Rev. E*, *77*, 056310.

[*James et al.* (2004)] James, M.R., S.J. Lane, B. Chouet, and J.S. Gilbert (2004), Pressure changes associated with the ascent and bursting of gas slugs in liquid-filled vertical and inclined conduits, *J. Volcanol. Geotherm. Res.*, *129*, 61–82.

[*James et al.* (2008)] James, M.R., S.J. Lane, and S.B.Corder (2008), Modelling the rapid near-surface expansion of gas slugs in low-viscosity magmas, In: Lane, S.J., Gilbert, J.S. (Eds.), *Fluid motion in volcanic conduits: A source of seismic and acoustic signals*, Geological Society, London, pp. 147–167. Special Publications.

[*James et al.* (2009)] James, M.R., S.J. Lane, L. Wilson, and S.B.Corder (2009), Degassing at low

magma-viscosity volcanoes: Quantifying the transition between passive bubble-burst and Strombolian eruption, *J. Volcanol. Geotherm. Res.*, *180*, 81–88.

[*Johnson* (2003)] Johnson, J.B. (2003), Generation and propagation of infrasonic airwaves from volcanic eruptions, *J. Volcanol. Geotherm. Res.*, *121*, 1–14.

[*Johnson* (2007)] Johnson, J.B. (2007), On the relation between infrasound, seismicity, and small pyroclastic explosions at Karymsky Volcano, *J. Geophys. Res.*, *112*, B08203.

[*Kinsler et al.* (1982)] Kinsler L.E., Frey A.R., Coppens A.B., and J.V. Sanders (1982), *Fundamentals of Acoustics*, 3rd Ed. (J.Wiley & Sons, Inc., New-York)

[*Kobayashi et al.* (2005)] Kobayashi, T., Y. Ida, and T. Ohminato (2005), Small inflation sources producing seismic and infrasonic pulses during the 2000 eruptions of Miyake-jima, Japan, *Earth Planet. Sci. Lett.*, *240*, 291–301.

[*Marchetti et al.* (2009)] Marchetti, E., M. Ripepe, A. J. L. Harris, and D. Delle Donne (2009), Tracing the differences between Vulcanian and Strombolian explosions using infrasonic and thermal radiation energy, *Earth Planet. Sci. Lett.*, *279*, 273–281.

[*McGonigle et al.* (2009)] McGonigle, A. J. S., A. Aiuppa, M. Ripepe, E. P. Kantzas, and G. Tamburello (2009), Spectroscopic capture of 1 Hz volcanic SO_2 fluxes and integration with volcano geophysical data, *Geophys. Res. Lett.*, *36*, L21309.

[*Mysels et al.* (1959)] Mysels, K. J., K. Shinoda, and S. P. Frankel (1959), *Soap Films, Studies of their Thinning and a Bibliography*, Pergamon, Oxford.

[*Ripepe et al.* (1996)] Ripepe, M., P. Poggi, T. Braun, and E. Gordeev (1996), Infrasonic waves and volcanic tremor at Stromboli, *Geophys. Res. Lett.*, *23*, 181–184.

[*Ripepe et al.* (2001)] Ripepe, M., S. Ciliberto, and M. Della Schiava (2001), Time constraints for modeling source dynamics of volcanic explosions at Stromboli, *J. Geophys. Res.*, *106*, 8713–8727.

[*Vergniolle and Brandeis* (1996)] Vergniolle, S., and G. Brandeis (1996), Strombolian explosions 1. A large bubble breaking at the surface of a lava column as a source of sound, *J. Geophys. Res.*, *101*, 20433–20447.

[*Vidal et al.* (2006)] Vidal, V., J.-C. Géminard, T. Divoux, and F. Melo (2006), Acoustic signal associated with the bursting of a soap film which initially closes an overpressurized cavity. Experiment and theory, *Eur. Phys. J. B 54*, 321–339.

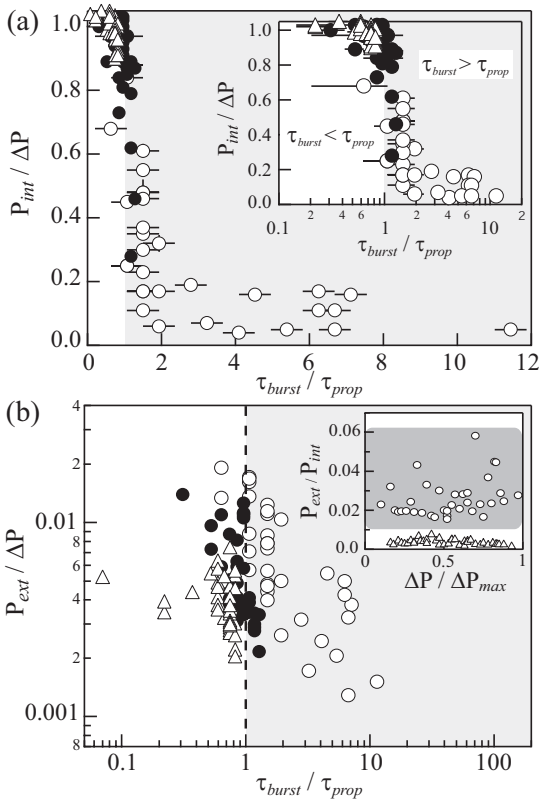

Figure 3: Normalized amplitude of the acoustic signal at bursting, inside (a) and outside (b) the cavity, as a function of the ratio between the bursting time τ_{burst}, and the propagation time τ_{prop}. P_{ext} is recorded at $r = 5$ cm from the cavity aperture. The light gray region indicates a slow rupture dynamics of the film ($\tau_{burst}/\tau_{prop} > 1$, same as Figure 2). *Insets:* (a) Semi-log plot of $P_{int}/\Delta P$ as a function of τ_{burst}/τ_{prop}. The efficiency of the bubble bursting to transmit pressure waves in the air drastically drops for slow rupture dynamics ($\tau_{burst}/\tau_{prop} > 1$). (b) Amplitude ratio P_{ext}/P_{int}. The most efficient energy partitioning occurs for the shorter tube (dark gray region). [Symbol,α]: [○,2]; [●,8]; [△,23].

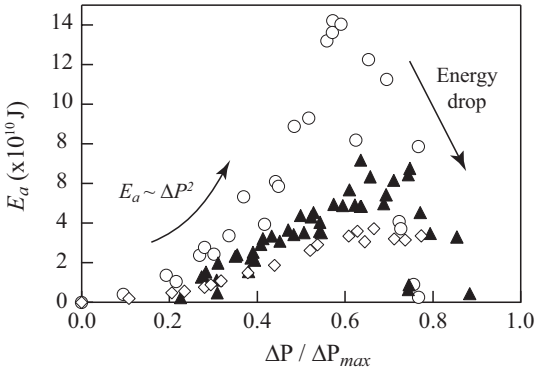

Figure 4: Acoustic energy E_a as a function of the initial overpressure ΔP (normalized to ΔP_{max}) for different lengths (same diameter $d = 8$ mm). All data represent the maximum pressure recorded outside over a series of ten measurements. We assume that this value corresponds to the signal recorded when the rupture time is negligible ($\tau_{burst}/\tau_{prop} < 1$). [Symbol,$\alpha$]: [○,2.5]; [▲,5]; [◇,6.9].